misdirected valency is invalid. Inspection of eq 3 shows that the off-axis $\sigma$ interaction *does* contribute to the d-orbital splitting, reducing the separation between $d_{xy}$ and $d_{yz,zx}$. Therefore, the obtained $\delta$ value is smaller than expected for no off-axis $\sigma$ interaction.

**Properties of Iron(II)- and Iron(III)-Thiolate Bondings.** The analogous $Fe^{II}$ complex $(Ph_4P)_2[Fe(SPh)_4]$ is well-known to be a successful synthetic model of the active site of reduced rubredoxin. The coordination geometries of the $Fe^{II}$ complex[14] and the rubredoxin active site[15] are similar to that of the $Co^{II}$ complex in that the S-Fe-S-C torsion angles are ca. 180°. Although the overall d-orbital splittings for the $Fe^{II}$ ions are not known, it is known that the ground d orbitals are $d_{z^2}$ well separated from $d_{x^2-y^2}$ for both.[14,18] This splitting pattern is identical to that of the $Co^{II}$ complex and suggests a substantial $\pi$ interaction between the $Fe^{II}$ ions and the thiolate sulfurs. The separations between $d_{z^2}$ and $d_{x^2-y^2}$ are, however, remarkably reduced compared with the separation in the $Co^{II}$ complex ($\mu$ = 4140 $cm^{-1}$): $\mu \geq 1000$[14] and $\approx$850 $cm^{-1}$ [18] were estimated for the $Fe^{II}$ model complex and reduced rubredoxin, respectively. (Although the $\mu$ value of the model complex is not known well, the value will not be very different from that of reduced rubredoxin.) The relatively small $\mu$ values suggest a weaker nature of the $Fe^{II}$-S $\pi$ interaction.

The occurrence of weaker $\pi$ interaction in iron(II)-sulfur bonding can also be evidenced by the recent spectroscopic study of $(Et_4N)_2[Fe(SC_6H_4\text{-}2\text{-}Ph)_4]$.[10] It was reported that this complex has a (strict) $S_4$ geometry with the S-Fe-S-C torsion angles being 47.6°, and hence the four $\pi$-bonding orbitals are directed to cancel with one another's effects on the e- and $t_2$-orbital splittings. We add to this that the $\pi$ interaction can affect the splittings nevertheless by allowing a mixing between $d_{x^2-y^2}$ and $d_{xy}$ (both d orbitals belong to the same representation B under $S_4$ symmetry). Therefore, if the $\pi$ interaction were enough strong, the d-orbital splitting pattern would be $d_{x^2-y^2} < d_{z^2} < d_{yz,zx} < d_{xy}$. However the actual $t_2$-orbital splitting is such that $d_{xy}$ is situated lower than $d_{yz,zx}$. This indicates that the $\pi$ interaction competes with the off-axis $\sigma$ interaction in the iron(II)-thiolate bonding.

The d-orbital splitting in an iron(III)-thiolate complex, $(Et_4N)[Fe(SC_6HMe_4)_4]$, was recently examined in detail.[8,9] In this complex, the S'-M-S-C torsion angles are all ca. 90° ($S_4$ symmetry).[31] Hence the d-orbital splitting pattern expected for strong $\pi$ interaction is $d_{x^2-y^2} < d_{z^2} < d_{yz,zx} < d_{xy}$. However the actual splitting pattern is $d_{z^2} < d_{x^2-y^2} < d_{xy} < d_{yz,zx}$, and both e- and $t_2$-orbital splitting patterns are opposite to the expected ones. Therefore the $\pi$ interaction between iron(III) and thiolate sulfur must be weak or even negligible as reported previously.[9]

In all likelihood, the findings about the cobalt(II)-thiolate bonding are easily understandable in the framework of the usual metal-ligand bonding scheme. Moreover, they compare well with previous molecular-orbital calculations,[6,7] though the calculations concerned iron thiolates. Thus the very weak $\pi$ interaction for iron(III)-thiolate bonding is instead perplexing. The reason for the discrepancy between the theoretical and experimental results on the iron(III)-thiolate bonding is not known and is left for a future study.

## Summary

The single-crystal ESR and susceptibility results have established significantly large ZFS and highly anisotropic $g$ values in the cobalt(II)-thiolate complex. It is concluded that these magnetic properties arise from the combination of the $D_{2d}$-type thiolate coordination and the strong $\pi$ interaction between cobalt(II) and thiolate sulfur. The finding of the strong $\pi$ interaction is especially exciting. This contrasts cobalt(II)-thiolate bonding with iron(II)-thiolate bonding, where the $\pi$ interaction is not very strong, and with iron(III)-thiolate bonding, where the $\pi$ interaction is very weak. The findings presented here and elsewhere[3-5,8-10] can be summarized as the following series of metal ions arranged according to their ability to form $\pi$ bonds with thiolate sulfur:

$$Fe^{III} < Fe^{II} < Co^{II} \sim Cu^{II}$$

Furthermore, the concept of misdirected valency seems to become more relevant in the reversed order.

**Acknowledgment.** We thank Dr. Hideki Masuda (Institute for Molecular Science, Okazaki, Japan) for the X-ray diffraction measurements. This work was partially supported by a Grant-in-Aid for Scientific Research from the Ministry of Education, Science and Culture, Japan.

**Registry No.** $(Ph_4P)_2[Co^{II}(SPh)_4]$, 57763-37-8.

(31) Millar, M.; Lee, J. F.; Koch, S. A.; Fikar, R. *Inorg. Chem.* **1982**, *21*, 4105-4106.

Contribution from the Inorganic Chemistry Laboratory, University of Oxford, South Parks Road, Oxford OX1 3QR, U.K.

# Applications of Two-Photon Spectroscopy to Inorganic Compounds. 2. Spectrum and Electronic Structure of $CsUO_2(NO_3)_3$

Trevor J. Barker, Robert G. Denning,* and Jonathan R. G. Thorne

*Received October 2, 1991*

The low-temperature two-photon absorption spectrum of a single crystal of $CsUO_2(NO_3)_3$ is reported. The spectrum is much simpler than the single-photon absorption; together they locate nine excited electronic states. The symmetry of these states is determined, and their accurate location enables an assignment of excited-state vibrational frequencies. Only the frequencies of the uranyl cation modes are significantly modified compared to the ground state. With this data set we have refined our model of the excited-state configurations and the perturbation of the equatorial field. The results confirm that the electronic structural model of the uranyl core is transferable, with only minor modifications, between the tetragonal field of four chloride ions in $Cs_2UO_2Cl_4$ and the trigonal field of the three nitrate ions in $CsUO_2(NO_3)_3$.

## Introduction

The single-photon electronic spectra of most uranyl compounds are extraordinarily complex. In part 1 of this series[1] we showed that the electronic excited states of $Cs_2UO_2Cl_4$ could be located much more readily using two-photon absorption spectroscopy (TPA) than by the familiar one-photon absorption spectroscopy (OPA). $Cs_2UO_2Cl_4$ crystallizes in a centrosymmetric space group, and as a result, the two experiments are largely complementary. TPA only enables transitions to the parity-conserving excited states and displays mainly the pure electronic transitions and totally symmetric progressions associated with them, while OPA shows the parity-changing transitions, which are exclusively induced by

(1) Barker, T. J.; Denning, R. G.; Thorne, J. R. G. *Inorg. Chem.* **1987**, *26*, 1721.

0020-1669/92/1331-1344$03.00/0 

**Table I.** OPA and TPA Selection Rules for $CsUO_2(NO_3)_3$[a]

| $D_{\infty h}$ | OPA | TPA | $D_{3h}$ | OPA | TPA | $D_3$ | OPA | TPA |
|---|---|---|---|---|---|---|---|---|
| $\Sigma_g^+$ | | (all) | $A_1'$ | | (all) | $A_1$ | | (all) |
| $\Sigma_g^-$ | $\mu_z$ | | $A_2'$ | $\mu_z$ | | $A_2$ | $z,\mu_z$ | |
| $\Pi_g$ | $\mu_x,\mu_y$ | $(xz)(yz)$ | $E''$ | $\mu_x,\mu_y$ | $(xz)(yz)$ | E | $x,y,\mu_x,\mu_y$ | $(1-z^2)$ |
| $\Delta_g$ | | $(1-z^2)$ | $E'$ | $x,y$ | $(1-z^2)$ | E | $x,y,\mu_x,\mu_y$ | $(1-z^2)$ |
| $\Phi_g$ | | | $A_1''$ | | | $A_1$ | | (all) |
| | | | $A_2''$ | $z$ | | $A_2$ | $z,\mu_z$ | |
| $\Gamma_g$ | | | $E'$ | $x,y$ | $(1-z^2)$ | E | $x,y,\mu_x,\mu_y$ | $(1-z^2)$ |

[a] $\mu_i$ are magnetic-dipole transition moments. (all) indicates intensity in all polarizations. $(1-z^2)$ indicates intensity in all polarizations except $(zz)$.

odd parity vibrations. We were able to locate and identify the symmetry of 13 of the 14 excited states present in the region below 33 000 $cm^{-1}$.

Here we apply the TPA technique to $CsUO_2(NO_3)_3$. In this compound the equatorial ligands which surround the linear uranyl ion form a trigonal array, as opposed to the near-tetragonal environment of the chloride ions in $Cs_2UO_2Cl_4$. Although the uranium site is not centrosymmetric, we shall see that the different selection rules for TPA, together with the relative insignificance of vibronic intensity, make the spectrum easier to interpret than the OPA.

The comparison of the spectra of these two compounds is valuable in testing the hypothesis that the influence of the equatorial ligands is a minor perturbation on the excited states. If this is correct, the electronic structural model of the uranyl ion should be transferable, with appropriate modifications, between the two coordination geometries. For this purpose it is essential to have a proper assignment of the excited-state symmetries and energies, in both tetragonal and trigonal ligand fields. In our OPA studies of $CsUO_2(NO_3)_3$ we were only able to observe the location of three electronic excited states directly, but another four were inferred from their vibronic structure.[2] We now show that the combination of OPA and TPA locates eight electronic origins directly and determines the position of a ninth within narrow limits. We then use the data to refine the model of the electronic structure which we developed some time ago.[3]

## Experimental Section

The experimental method has been described elsewhere.[1] TPA is detected by luminescence excitation and photon counting. The samples were mounted in an Oxford Instruments Model CF204 continuous-flow cryostat. Luminescence was detected at right angles to the incident beam and passed through a wide band interference filter, with a 50-nm spectral band-pass centered at 500 nm. When red laser light was in use, additional green or blue glass filters were added. For each dye range the emission intensity is divided by the square of the energy detected by the reference photodiode. This method can be criticized on the grounds that the laser pulse length is shorter at the ends of the dye range and so the pulse intensity is relatively higher than indicated by the pulse energy. We were unable to measure the temporal properties of the laser output and so have not corrected for this effect; it introduces some uncertainty into the relative intensity of spectral features near the limits of a laser dye wavelength range. The scaling of the relative intensities for different dye segments has been done in such a way as to make the Franck–Condon factors in the progressions appear reasonable and where appropriate to match those observed in OPA. OPA measurements were made in transmission on a McPherson RS-10 spectrophotometer as described previously.[2]

## Background

Crystals of $CsUO_2(NO_3)_3$ belong to the trigonal space group $R3c$ ($D_{3d}^6$).[4] The site symmetry of the uranium atom is $D_3$, there being two enantiomeric molecules within the unit rhombohedral cell. Although it has been claimed that the isomorphous rubidium salt shows a small monoclinic distortion,[5] a recent high-precision X-ray study confirms that the space group is trigonal.[6] In the rubidium salt the three bidentate nitrate groups, which form the equatorial coordination of the uranyl ion, are canted by about 5° from the equatorial plane to form a chiral array, but the predominant local symmetry is not far from $D_{3h}$. The uranyl groups separated by alkali-metal cations form linear chains along the $c$-axis, in which uranium, oxygen, and alkali-metal atoms all lie on a 3-fold axis. In the cesium salt studied here the U–U distance in this direction is 976 pm. In the nearest-neighbor chain, which is only 556 pm away, the uranyl group is displaced by 325 pm along $c$, giving a U–U distance of 645 pm. This arrangement places the coordinated oxygen atom of the nitrate group in one molecular anion about 350 pm along the $c$-axis direction from an equivalent oxygen atom in a molecule in the adjacent chain. This is the most significant contact between the molecular anions, so it is to be expected that vibrational factor group splittings of the internal modes will predominantly involve nitrate vibrations. These

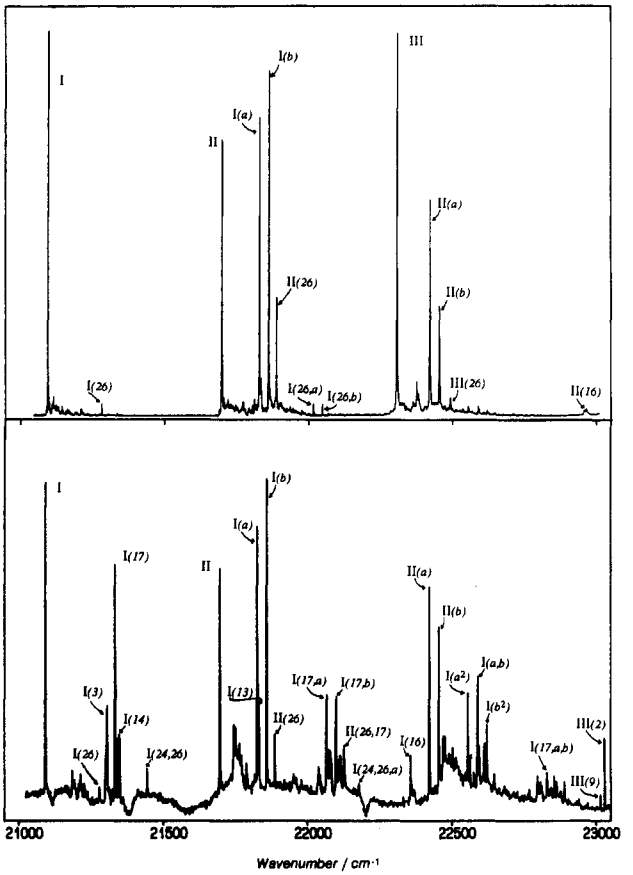


**Figure 1.** Two-photon absorption (top) and lower section $\pi$-polarized single-photon absorption (bottom) of a crystal of $CsUO_2(NO_3)_3$ at ~5 K. Origin bands are indicated by Roman numerals. Numbers in parentheses are the modes of Figure 7 and Table II; superscripts give the number of quanta if >1. a and b are the progression-forming modes composed of $\nu_1$ and $\nu_6$. ph indicates a group of low frequency, <120 $cm^{-1}$, phonon modes, and $\{a/b\}^n$ denotes a group in which the sum of $a$ and $b$ quanta is $n$.

(2) Denning, R. G.; Foster, D. N. P.; Snellgrove, T. R.; Woodwark, D. R. *Mol. Phys.* **1979**, *37*, 1089.
(3) Denning, R. G.; Snellgrove, T. R.; Woodwark, D. R. *Mol. Phys.* **1979**, *37*, 1109.
(4) Barclay, G. A.; Sabine, T. M.; Taylor, J. C. *Acta Crystallogr.* **1965**, *19*, 205.
(5) Kvapil, J.; Kvapil, J.; Tethal, T. *J. Cryst. Growth* **1971**, *10*, 279.
(6) Zalkin, A.; Templeton, L. K.; Templeton, D. H. *Acta Crystallogr.* **1989**, *C45*, 810.

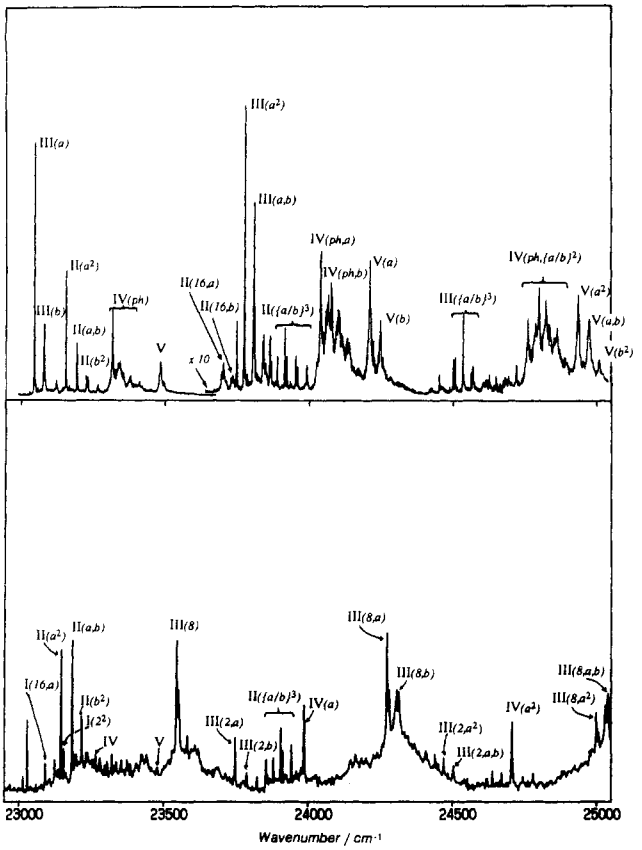


**Figure 2.** See caption for Figure 1.

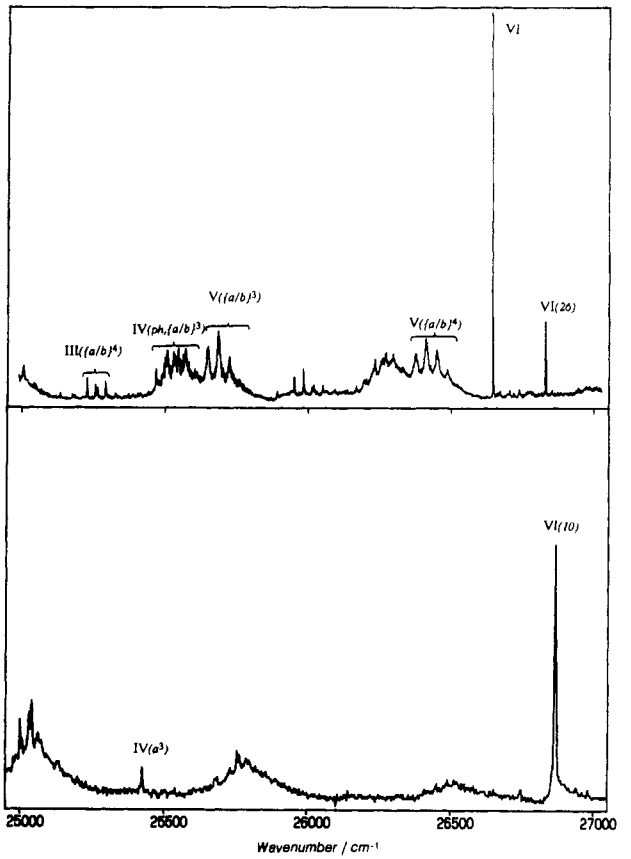


**Figure 3.** See caption for Figure 1.

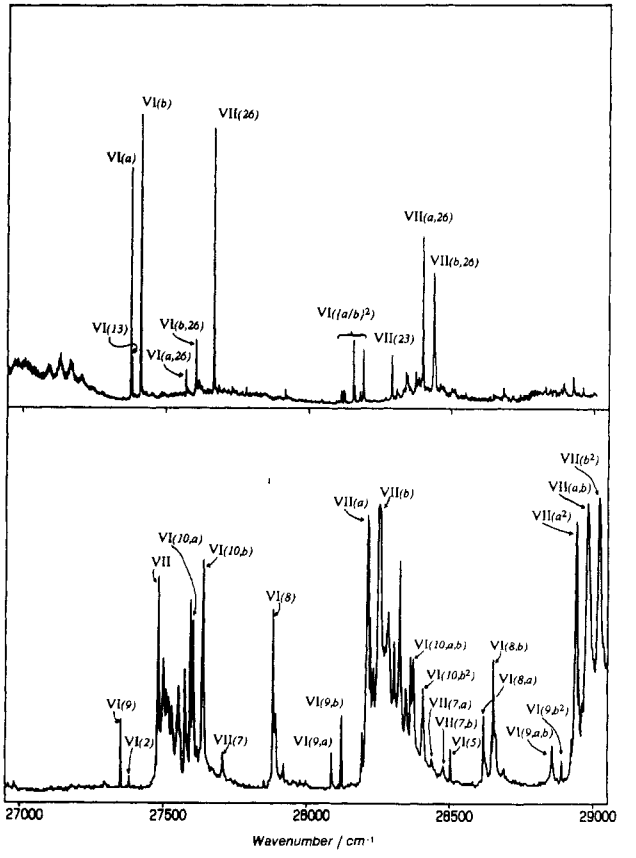


**Figure 4.** See caption for Figure 1.

modes should be most prominent in any dispersion with wave vector that is observed in the vibronic structure.

The selection rules for OPA and TPA are summarized in Table I, which includes both the rigorous site symmetry group $D_3$ and the idealized group $D_{3h}$. The TPA selection rules follow the work of Bader and Gold[7] with the constraints implied by the use of a single laser color.

## Results

Figures 1–6 show the TPA spectrum of $CsUO_2(NO_3)_3$ at ~5 K, together with the corresponding OPA spectrum polarized parallel to the *c*-axis. Measurements have also been made on the samples in which the uranyl group contains greater than 90% oxygen-18. The perpendicularly polarized OPA spectrum is not useful for the purpose of a general comparison because it is too intense in many spectral regions to be recorded properly on crystals of manageable thickness.[2] We have been unable to observe any significant polarization in the TPA spectrum, despite the implications of Table I. We believe this is a consequence of measuring the TPA by means of luminescence excitation. In contrast to a transmission measurement, light, which has become depolarized by scattering from the mounting plate and from the faces and imperfections in the crystal contributes to the excitation. In particular the crystals showed signs of surface damage where the focused beam was incident, so the light scattered from the damaged area may be sufficiently depolarized to account for our observations.

## Structure of the Main Progressions

The figures show obvious progressions throughout both OPA and TPA spectra with an interval of about 740 $cm^{-1}$. However in almost all cases the number of features increases by one in each new member of the progression. We have established[2] that this arises from the near degeneracy of the $UO_2$ symmetric stretching mode $\nu_1$ and the mode in which the chelate angles between the bridging oxygen atoms of all three nitrate ligands deform in phase. This mode is labeled $\nu_6$. A diagram of all the internal modes is shown in Figure 7; Table II gives their frequencies. An interaction force constant describes the mixing of these two modes.

Our analysis in ref 2 showed how the relative intensities of the components of each element of the OPA progression based on the

(7) Bader, T. R.; Gold, A. *Phys. Rev.* **1968**, *A171*, 997.

**Table II.** Normal Modes of $[UO_2(NO_3)_3]^-$

| notation | sym ($D_{3h}$) | mode description | freq/cm$^{-1}$ groundstate | freq/cm$^{-1}$ excited states |
|---|---|---|---|---|
| $\nu_1$ | $A_1'$ | $UO_2$ sym str | 880 | 734 (I); see Tables VI and VII |
| $\nu_2$ | $A_2''$ | $UO_2$ asym str | 956 | 732 (II), 721 (III), 736 (VI) |
| $\nu_3$ | E′ | $UO_2$ bend | 265 | 214 (I), 203 (VII) |
| $\nu_4$ | $A_1'$ | $NO_3$ term O str [s][a] | 1510 | |
| $\nu_5$ | $A_1'$ | $NO_3$ bridge O sym str [s] | 1023 | 1023 (VI) |
| $\nu_6$ | $A_1'$ | $NO_3$ bridge O bend [s] | 749 | 766 (I); see Tables VI and VII |
| $\nu_7$ | $A_1'$ | Equat ring breath [s] | | 227.4 (VII) |
| $\nu_8$ | $A_2'$ | $NO_3$ bridge O asym str [s] | 1245 | 1242 (II), 1237 (III), 1238 (VI) |
| $\mu_9$ | $A_2'$ | Term N–O wag [s] | 711 | 706 (III), 704 (VI) |
| $\nu_{10}$ | $A_2'$ | $NO_3$ rock [s] | | 220 (VI) |
| $\nu_{11}$ | E′ | $NO_3$ term O str [a] | 1540 | |
| $\nu_{12}$ | E′ | $NO_3$ bridge O sym str [a] | 1020 | |
| $\nu_{13}$ | E′ | $NO_3$ bridge O bend [a] | 739 | 739 (I), 741 (VI) |
| $\nu_{14}$ | E′ | Equat ring breath [a] | | 255 (I), 258 (II), 252 (VII) |
| $\nu_{15}$ | E′ | Term N–O wag [a] | 711 | |
| $\nu_{16}$ | E′ | $NO_3$ bridge O asym str [a] | 1268 | 1267 (I), 1266/1273 (II) |
| $\nu_{17}$ | E′ | $NO_3$ rock [a] | | 242 (I), 242 (II), 237 (VII) |
| $\nu_{18}$ | E′ | $NO_3$ wag [a] | | |
| $\nu_{19}$ | $A_1''$ | $NO_3$ oop twist [s] | | |
| $\nu_{20}$ | $A_2''$ | Term N–O oop bend [s] | 806 | 804 (I) |
| $\nu_{21}$ | $A_2''$ | $NO_3$ oop rock [s] | | |
| $\nu_{22}$ | $A_2''$ | $NO_3$ oop bend [s] | | |
| $\nu_{23}$ | E″ | Term N–O oop bend [a] | 806 | 806 (VII) |
| $\nu_{24}$ | E″ | $NO_3$ oop rock [a] | | 164 (I) |
| $\nu_{25}$ | E″ | $NO_3$ oop bend [a] | | |
| $\nu_{26}$ | E″ | $UO_2$ rock | 222 | 189 (I), 189 (II), 186 (III), 186 (VI), 186 (VII) |

[a] [s] and [a] denote symmetric and asymmetric combinations of individual nitrate modes.

**Table III.** Repeat Intervals on Origin III[a]

| assgnt | freq/cm$^{-1}$ obs | freq/cm$^{-1}$ calc | intensity obs | intensity calc | repeat intervals/cm$^{-1}$ | |
|---|---|---|---|---|---|---|
| III(0,0) | 22 307 | 22 309 | | | | |
| III(1,0) | 23 037 | 23 037 | 0.77 | 0.77 | (0,0) + 730 | |
| III(0,1) | 23 071 | 23 070 | 0.23 | 0.23 | | (0,0) + 764 |
| III(2,0) | 23 764 | 23 764 | 0.59 | 0.59 | (1,0) + 727 | |
| III(1,1) | 23 796 | 23 797 | 0.35 | 0.36 | (0,1) + 725 | (1,0) + 759 |
| III(0,2) | 23 830 | 23 830 | 0.06 | 0.05 | | (0,1) + 759 |
| III(3,0) | 24 490 | 24 491 | 0.40 | 0.46 | (2,0) + 726 | |
| III(2,1) | 24 524 | 24 525 | 0.38 | 0.41 | (1,1) + 728 | (2,0) + 760 |
| III(1,2) | 24 558 | 24 558 | 0.17 | 0.12 | (0,2) + 728 | (1,1) + 762 |
| III(0,3) | 24 591 | 24 591 | 0.05 | 0.01 | | (0,2) + 761 |
| III(4,0) | 25 219 | 25 219 | 0.30 | 0.35 | (3,0) + 729 | |
| III(3,1) | 25 248 d | 25 252 | 0.38 | 0.42 | (2,1) + 724 | (3,0) + 758 |
| III(2,2) | 25 284 | 25 285 | 0.26 | 0.19 | (1,2) + 726 | (2,1) + 760 |
| III(1,3) | 25 318 | 25 318 | 0.06 | 0.04 | (0,3) + 727 | (1,2) + 760 |
| III(5,0) | 25 946 | 25 946 | 0.26 | 0.27 | (4,0) + 727 | |
| III(4,1) | 25 977 | 25 979 | 0.36 | 0.40 | (3,1) + 729 | (4,0) + 758 |
| III(3,2) | 26 012 d | 26 013 | 0.25 | 0.24 | (2,2) + 728 | (3,1) + 764 |
| III(2,3) | 26 044 | 26 046 | 0.13 | 0.07 | (1,3) + 726 | (2,2) + 760 |

[a] Figures in parentheses are the number of quanta of modes a and b, respectively. Intensities were assumed proportional to peak height. They have been normalized so that the sum of the intensities in any one repeat is unity. Peaks marked "d" are doubled. The quoted intensity is the sum of the two components.

**Table IV.** Repeat Intervals on Origin VI for $CsU^{16}O_2(NO_3)_3$[a]

| assgnt | freq/cm$^{-1}$ obs | freq/cm$^{-1}$ calc | intensity obs | intensity calc | repeat intervals/cm$^{-1}$ | |
|---|---|---|---|---|---|---|
| VI(0,0) | 26 644 | 26 644 | | | | |
| VI(1,0) | 27 381 | 27 381 | 0.42 | 0.42 | (0,0) + 737 | |
| VI(0,1) | 27 415 | 27 415 | 0.58 | 0.58 | | (0,0) + 771 |
| VI(2,0) | 28 118 d | 28 118 | 0.17 | 0.18 | (1,0) + 737 | |
| VI(1,1) | 28 151 | 28 152 | 0.48 | 0.49 | (0,1) + 736 | (1,0) + 770 |
| VI(0,2) | 28 186 | 28 186 | 0.35 | 0.33 | | (0,1) + 771 |
| VI(3,0) | 28 856 | 28 855 | 0.08 | 0.08 | (2,0) + 738 | |
| VI(2,1) | 28 891 d | 28 889 | 0.36 | 0.31 | (1,1) + 740 | (2,0) + 773 |
| VI(1,2) | 28 924 | 28 923 | 0.39 | 0.42 | (0,2) + 738 | (1,1) + 773 |
| VI(0,3) | 28 959 | 28 957 | 0.17 | 0.19 | | (0,2) + 773 |

[a] For notation see Table III.

**Table V.** Repeat Intervals on Origin VI for $CsU^{18}O_2(NO_3)_3$[a]

| assgnt | freq/cm$^{-1}$ obs | freq/cm$^{-1}$ calc | intensity obs | intensity calc | repeat intervals/cm$^{-1}$ | |
|---|---|---|---|---|---|---|
| VI(0,0) | 26 656 | 26 656 | | | | |
| VI(1,0) | 27 363 m | 27 363 | 0.86 | 0.87 | (0,0) + 707 | |
| VI(0,1) | 27 414 | 27 414 | 0.14 | 0.13 | | (0,0) + 758 |
| VI(2,0) | 28 072 m | 28 070 | 0.67 | 0.76 | (1,0) + 709 | |
| VI(1,1) | 28 120 | 28 121 | 0.29 | 0.22 | (0,1) + 706 | (1,0) + 757 |
| VI(0,2) | 28 171 | 28 171 | 0.03 | 0.02 | | (0,1) + 757 |
| VI(3,0) | 28 777 | 28 777 | 0.74 | 0.67 | (2,0) + 706 | |
| VI(2,1) | 28 828 | 28 828 | 0.26 | 0.29 | (1,1) + 709 | (2,0) + 757 |

[a] For notation see Table III. Peaks marked "m" appear to be multiple features. Only the largest component of each was measured, so the quoted values may be underestimates.

first excited state, I, could be approximately reproduced by a simple model. The mean of the two frequencies in the first repeat of the origin was taken as a constant, and the experimental data were fitted to two parameters, one describing the difference between the frequencies of the uncoupled modes and the other the magnitude of their coupling. The intensity of each component is calculated from the amplitude of the $UO_2$ symmetric stretching mode contained in it, since it is primarily this atomic displacement which is induced by the electronic excitation.

It is much easier to measure the relative intensities of the components of the progression in TPA, because the spectrum is relatively uncluttered by the vibronically induced intensity which complicates the OPA (Figures 1 and 2). Tables III and IV demonstrate the success of this analysis for progressions in TPA formed on the electronic origins III and VI. The agreement between the observed and calculated frequencies and intensities is quite remarkable. The intensities on origin VI in the corresponding $^{18}O$ spectrum are also very successfully reproduced by modifying the value of $\nu_1^0$ but leaving the other parameters unchanged; see Table V.

Table VI summarizes the results of this analysis for four different electronic origins. Notice that the nitrate frequency, $\nu_6^0$, is relatively insensitive to the nature of the electronic excited state

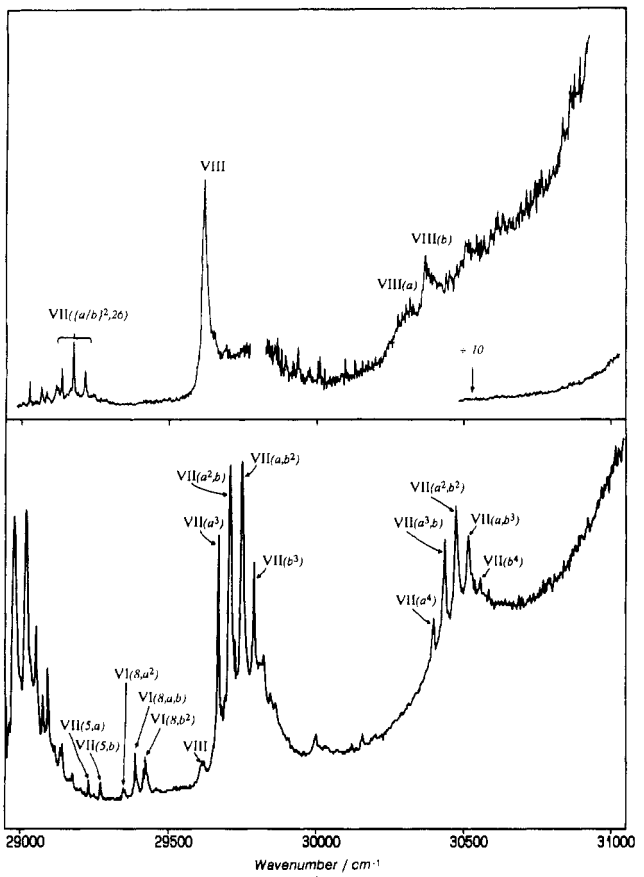


**Figure 5.** See caption for Figure 1.

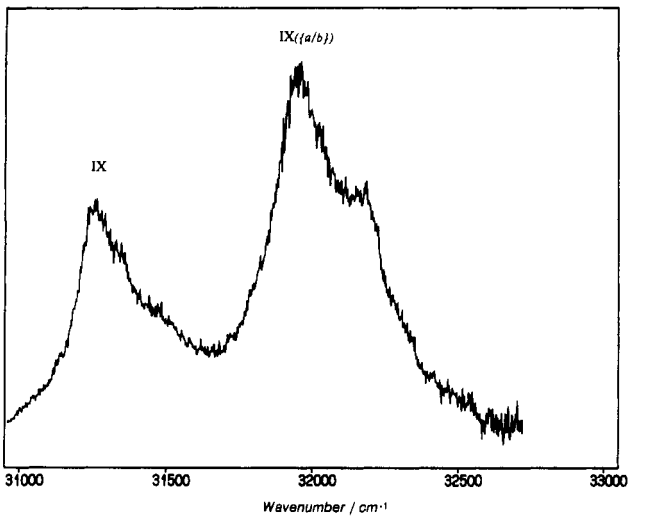


**Figure 6.** Two-photon absorption spectrum. Notation is as for figure 1.

**Table VI.** Uncoupled Frequencies of Progression-Forming Modes ($cm^{-1}$)

| origin | expt | $\nu_1^0$ | $\nu_6^0$ | $\delta/cm^{-1}$ [a] |
|---|---|---|---|---|
| I | OPA | 750 | 750 | 16 |
| I | OPA ($^{18}O$) | 708 | 750 | 16 |
| II | TPA | 738 | 751 | 15 |
| III | TPA | 735 | 753 | 14 |
| VI | TPA | 757 | 751 | 17 |
| VI | TPA ($^{18}O$) | 714 | 751 | 17 |

[a] Mode coupling parameter.

with a frequency very close to the ground-state value, 749 $cm^{-1}$, whereas the $UO_2$ stretching frequency, $\nu_1^0$, changes significantly from state to state. The magnitude of the interaction force constant correlates well with that of $\nu_1^0$. The U–O stretching

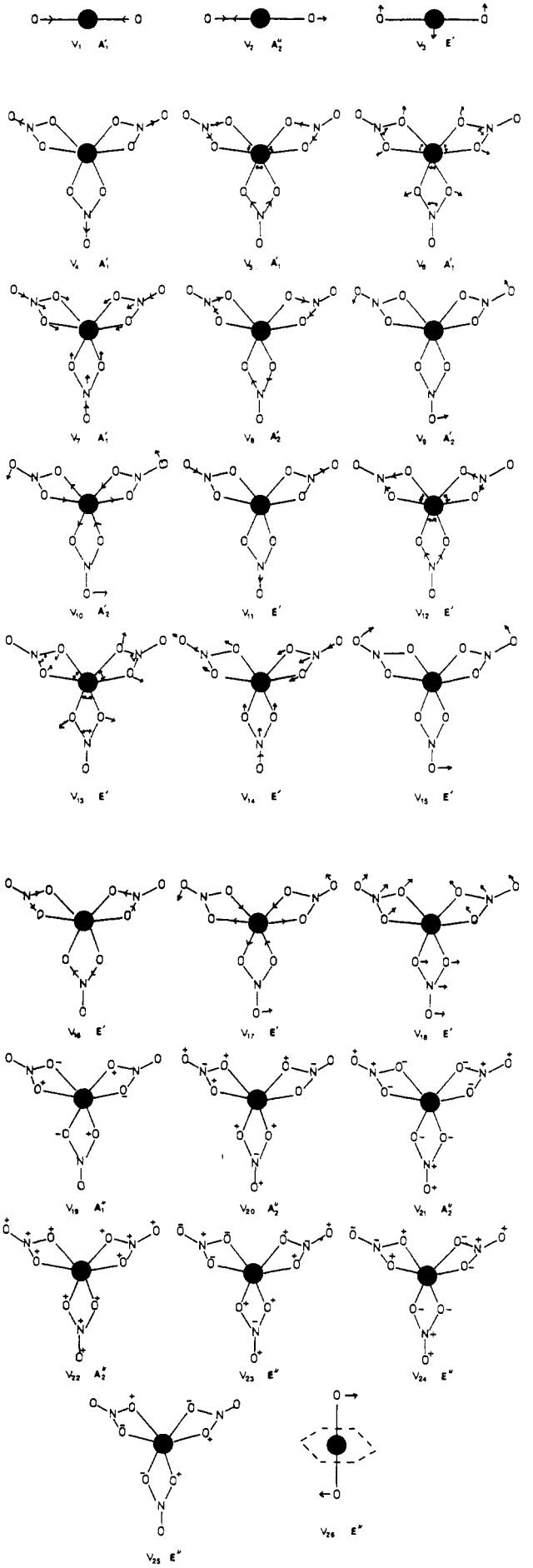

**Figure 7.** Normal modes of the $[UO_2(NO_3)_3]^-$ ion.

**Table VII.** Observed Origins in $CsUO_2(NO_3)_3$

| origin | sym $D_{\infty h}$ | sym $D_{3h}$ | energy/ $cm^{-1}$ | repeat intervals/ $cm^{-1}$ | | moment/ $\mu_B$ |
|---|---|---|---|---|---|---|
| I | $\Pi_g$ | E″ | 21 089.6 | 734 | 766 | 0.01 |
| II | $\Pi_g$ | E′ | 21 694 | 728 | 761 | 1.1 |
| III | $\Phi_g$ | $A_1$″ | 22 307 | 730 | 764 | |
| IV | $\Phi_g$ | $A_2$″ | 23 265[a] | 721 | 759 | |
| V | $\Delta_g$ | E′ | 23 474 | 724 | 761 | ~0.3[b] |
| VI | $\Phi_g$ | $A_1$″ | 26 644 | 737 | 771 | |
| VII | $\Phi_g$ | $A_2$″ | 27 480 | 730 | 771 | |
| VIII | $\Gamma_g$ | E′ | 29 618 | 700 | 752 | >0 |
| IX | $\Delta_g$ | E′ | 31 262 | ~690 | | >0 |

[a] Origin not clearly observed; see text for uncertainty in position. [b] Inferred from data on $NaUO_2(CH_3COO)_3$ in ref 2.

frequency varies inversely with the bond length in the electronic ground state of a number of uranyl compounds,[8] so the values of $\nu_1^0$ should indicate differences in the U–O equilibrium bond length in the electronic excited states. Those states with low values of $\nu_1^0$ and longer U–O bonds have significantly lower interaction forces coupling the oxygen displacements to those of the equatorial ligand oxygen atoms.

Armed with this analysis of the progression structure, the identification of electronic origin bands now becomes straightforward. It is also easy to understand why the complexity of the spectrum increases rapidly with increasing energy, because every spectral feature acquires an additional component after each repeat interval. Because of the interaction of $\nu_1$ and $\nu_6$, the mode labels are arbitrary; so in Figures 1–6 we use the labels a and b in order of increasing energy.

**Electronic Excited States**

The observed electronic excited states are summarized in Table VII. Their symmetries may be deduced, in most cases, from the combination of their polarizations in OPA and the selection rules in TPA. We now examine each origin in turn.

**Origin I.** Origin I was analyzed quite fully in ref 2. It has mainly magnetic dipole character in OPA implying $E''(D_{3h})$ as the predominant excited-state symmetry, although a very weak electric dipole intensity shows the influence of the actual $D_3$ site symmetry. It is this combination of transition mechanisms which accounts for the very large disymmetry factor in the natural circular dichroism of the equivalent transition in $NaUO_2(CH_3COO)_3$. The magnetic circular dichroism (MCD) spectrum establishes the presence of a very small magnetic moment, 0.01 $\mu_B$. The polarization of the OPA vibronic structure supports the assignment, and the strong TPA intensity conforms to the predictions of Table I.

**Origin II.** This origin is observed in TPA and in *both* OPA polarizations. The sharpness of the lines allows an accurate determination of the Zeeman splitting, which corresponds to a magnetic moment of 1.1 $\mu_B$. All the sharp vibrational structure built on this origin in Figures 1 and 2 can be identified by means of this splitting. This degeneracy and the very strong intensity of the transition in the OPA-$\sigma$ (perpendicular) polarization requires $E(D_3)$ symmetry, with E′ parentage in $D_{3h}$ rather than E″. Nevertheless the origin bands are clear and sharp, if weak, in the OPA-$\pi$ (parallel) polarization shown in Figure 1. $D_3$ symmetry requires E excited states observed in this polarization to be magnetic dipole allowed, but this is inconsistent with the E′ parentage in $D_{3h}$. In a later section we show how this intensity can be accounted for by an exciton coupling mechanism.

**Origin III.** The third excited state is not directly located in OPA as expected from its $A_1''(D_{3h})$ symmetry; its position had to be determined approximately using vibrational sidebands.[2] However this feature appears strongly in the TPA spectrum (Figure 1) as expected from the selection rules in Table I, at 22 307 $cm^{-1}$. This allows the assignment of the feature at 23 029 $cm^{-1}$ in the OPA-$\pi$ spectrum, which has a large oxygen-18 negative isotope shift, to the $UO_2$ asymmetric stretching mode with a frequency of 721 $cm^{-1}$. This mode has the required $a_2$ symmetry in $D_3$ to enable intensity in this polarization. The OPA features do not exhibit a Zeeman splitting as expected for a nondegenerate state.

**Origin IV.** The proper location of this origin presents the most difficult part of the analysis. The TPA spectrum shows a new region of absorption beginning at 23 307 $cm^{-1}$, which is not a part of a previous progression. This has the expected 10-$cm^{-1}$ positive oxygen-18 isotope shift characteristic of structure built on a new origin, and it appears as a double feature in the repeated element near 24 030 $cm^{-1}$ in the manner anticipated in our discussion of the progressions.

The main features of the electronic structure[3] lead to the expectation that a state of $A_2''(D_{3h})$ symmetry should accompany the $A_1''$ state responsible for origin III. The electronic transition to a state of this symmetry is forbidden in TPA but should be allowed in the OPA-$\pi$ spectrum. For example, another state of this symmetry, VII, is responsible for the strong OPA-$\pi$ band at 27 480 $cm^{-1}$. Unfortunately, there is no obvious origin band in the OPA-$\pi$ spectrum at this point although there are weak features at 23 265, 23 279, 23 286, and 23 305 $cm^{-1}$. They are sufficiently weak to make it difficult to be certain that they are not part of the complex low-frequency phonon structure built on lower frequency origins, whose higher progression members occur in this region.

The best evidence for the location of origin IV comes from a well-defined OPA-$\pi$ transition at 23 985 $cm^{-1}$ with an obvious repeat at 24 706 $cm^{-1}$ (Figure 2). This shows no Zeeman splitting and has an oxygen-18 isotope shift of −25 $cm^{-1}$ typical of one quantum of either the $UO_2$ symmetric or asymmetric stretching modes. In the $\pi$-polarization its vibronic symmetry must be $A_2(D_3)$. Assuming that the origin has the $A_2(D_3)$ symmetry required by the theoretical model, the mode responsible for this band must be $\nu_1$, the $a_1$ totally symmetric $UO_2$ stretch. This band has a repeat interval of 721 $cm^{-1}$, three members of the progression in $\nu_1$ being observed, which is identical to the interval in the structure identified as built on origin IV in the TPA spectrum. It follows that origin IV must occur at 23 264 $cm^{-1}$, a value which corresponds well to the weak OPA-$\pi$ feature at 23 265 $cm^{-1}$.

This OPA band is notably weak compared with its first repeat, in contrast to earlier origins where the intensity falls throughout the progression (Figure 1). Also the length of the progression on this origin extends to at least six members in TPA (Figures 2–4) compared with virtual disappearance of the progression on origin II after four members. Both of these points suggest a larger Huang–Rhys factor for this transition, which implies a greater change in the excited-state bond length relative to the ground state. This fits the lower frequency of $\nu_1$, 721 $cm^{-1}$ on origin IV, compared to 734 $cm^{-1}$ on origin I and 728 $cm^{-1}$ on origin II, and so we believe that the low intensity of the origin band is credible.

If this assignment of the position of origin IV is correct, there is then an interval of about 42 $cm^{-1}$ between it and the beginning of the vibronic structure observed in the TPA spectrum. The intervals in these low-frequency vibrations do not correspond well to those observed on allowed origins both in TPA and OPA (see below), where the dominant features occur at 22, 49, 74, 94, and 114 $cm^{-1}$. This point would seem to argue against the validity of the assignment. However, because the TPA intensity on origin IV must be vibronic, different modes will dominate the low-frequency vibrational structure from those that appear on allowed origins. For example the low-frequency structure on origin II near 21 700 $cm^{-1}$ in the OPA-$\pi$ spectrum (Figure 1) must have vibronically induced intensity, and the first significant band in the spectrum occurs 48 $cm^{-1}$ above the origin.

**Origin V.** The TPA spectrum shows a further rather broad feature at 23 474 $cm^{-1}$. It corresponds to an intense OPA-$\sigma$ band at the same energy, which is not part of an earlier progression, and shows the same progression interval of 724 $cm^{-1}$ in both experiments. It is at this point that the MCD spectrum of Brint and McCaffery[9] shows evidence of the start of a new progression

(8) Bartlett, J. R.; Cooney, R. P. *J. Mol. Struct.* **1989**, *193*, 295.

(9) Brint, P.; McCaffery, A. J. *Mol. Phys.* **1973**, *25*, 311.

with a nonzero first-order magnetic moment, an "*A*" term in the nomenclature of MCD. The spectrum of $NaUO_2(CH_3COO)_3$, which can be closely compared with that of $CsUO_2(NO_3)_3$, also shows evidence of an analogous transition giving a new MCD *A* term in this region.[2] The TPA origin repeats strongly for at least five quanta; the progression interval of 724 $cm^{-1}$ is noticeably larger than the 721 $cm^{-1}$ found on origin IV. The magneto-optic data, taken with the OPA polarization indicates the same $E'(D_{3h})$ as origin II. There is a weak band at 23 474 $cm^{-1}$ in OPA-$\pi$ (Figure 2), which may be magnetic dipole allowed by the same mechanism which allows origin II to appear in this polarization (see below).

**Origins VI and VII.** These are easily identified. The former with $A_1(D_3)$ symmetry is allowed in TPA but forbidden in OPA (Figure 3). The OPA spectrum shows a strong vibronic feature 220 $cm^{-1}$ above the origin, which we will discuss later. Origin VII, with $A_2$ symmetry is allowed in the OPA-$\pi$ polarization, but forbidden in TPA. However the $E''(D_{3h})$ rocking mode $\nu_{26}$ appears strongly in the TPA spectrum.

**Origins VIII and IX.** In the OPA-$\sigma$ spectrum very strong absorption sets in near 29 600 $cm^{-1}$ making the crystal effectively opaque. This appears to correspond to the onset of a strong progression in the absorption spectrum of $(Bu_4N)UO_2(NO_3)_3$ in a polymer matrix, near 29 325 $cm^{-1}$, with $\epsilon_{max} \sim 150$ $mol^{-1}$ $cm^{-1}$ $dm^3$, reported by Brint and McCaffery.[9] Their MCD results also show the presence of an *A* term in this region. In TPA the new band shows clearly as a strong broad feature at 29 618 $cm^{-1}$ (Figure 6). It has a $^{18}O$ isotope shift of +13 $cm^{-1}$ as expected for an electronic origin and shows evidence of a doubled repeat at 30 317 and 30 370 $cm^{-1}$. This suggests a $UO_2$ symmetric stretch of 700 $cm^{-1}$, with the corresponding nitrate mode, $\nu_6$, at 752 $cm^{-1}$. The repeat features are sharper in the $^{18}O$ spectrum, where the intervals are 669 and 754 $cm^{-1}$, confirming the assignment.

The strong OPA-$\sigma$ intensity implies $E'(D_{3h})$ symmetry, and we can expect the exciton coupling mechanism, discussed below in the context of origin II, to provide magnetic dipole intensity in the OPA-$\pi$ spectrum. It appears clearly in Figure 5 as a broad feature at 29 616 $cm^{-1}$, but the rise in the broad background absorption obscures the next member of the progression.

Figure 6 shows another large increase in TPA with strong absorption defining a very broad peak at 31 262 $cm^{-1}$. There is an $^{18}O$ isotope shift of about +15 $cm^{-1}$ indicating that this is origin IX. There is a repeat at about 31 960 $cm^{-1}$ which is too broad to show the usual doubling, but the interval of 700 $cm^{-1}$ implies that this transition is of the same type as all the previous ones, having the same effect on the uranium–oxygen bond. Brint and McCaffery[9] report an even more intense transition, with $\epsilon_{max} \sim 250$ $mol^{-1}$ $cm^{-1}$ $dm^3$, in their polymer solutions at 31 120 $cm^{-1}$, with a MCD *A* term which indicates an excited state with a first-order magnetic moment. In their spectrum this origin carries a progression of about six members. In the light of its magnetic moment and large intensity we can also assign this state $E'(D_{3h})$ symmetry.

**An Exciton Mechanism for Magnetic Dipole Intensity.** We now return to the anomalous intensity in the OPA-$\pi$ spectrum of origin II, which implies magnetic dipole intensity for a state of $E(D_3)$ symmetry but which is inconsistent with the $E'(D_{3h})$ parentage required by the strong electric dipole intensity in OPA-$\sigma$. Figure 1 shows the OPA-$\pi$ intensity in origin II is about 80% of that in origin I, which has been shown to be magnetic dipole allowed[2] as anticipated from its $D_{3h}$ parentage. It is not possible to argue that the magnetic dipole intensity in origin II is acquired by a second-order interaction with origin I, via a perturbation of $D_3$ symmetry, because this would mix much of the strong electric dipole perpendicular intensity in origin II into origin I, and that is not observed. The same argument may be used to dismiss the role of electric quadrupole intensity, which in this polarization would also be confined to $E''(D_{3h})$ excited states.

The dilemma can be resolved by noting that the true symmetry is that of the factor group, $D_{3d}$. In this group $E_g$ excited-state symmetry can account both for the OPA magnetic dipole intensity induced by that component of the magnetic field of the radiation polarized perpendicular to the 3-fold axis and also for the TPA intensity, which is of course confined to excited states of even parity. In the factor group the OPA electric dipole intensity in the $\sigma$-polarization arises from the in-phase combination of the electric dipole transition moments of the two molecules in the rhombohedral unit cell polarized perpendicular to $C_3$, giving an exciton state of $E_u$ symmetry, while the out-of-phase combination of these moments generates a rotation of charge about an axis perpendicular to $C_3$ and magnetic dipole intensity in the exciton state of $E_g$ symmetry.

To quantify this hypothesis, the relative intensities in the two polarizations can be estimated and compared to the predictions of a simple exciton or coupled-oscillator model. The large, 645 pm, separation of the closest uranium atoms compared to the localization length, say 200 pm, of transitions within the uranyl group suggests that the magnetic dipole transition moments can be calculated on the basis of two-point electric dipole transition moments centered on the uranium atoms.

Origin II at 21 694 $cm^{-1}$ in the $\pi$-polarization has a maximum molar extinction coefficient, $\epsilon_{max}$, of 0.79 $mol^{-1}$ $cm^{-1}$ $dm^3$ and a fwhm line width of 1.6 $cm^{-1}$, from which we calculate an oscillator strength of $5.85 \times 10^{-9}$. Unfortunately, the origin band is far too intense in the $\sigma$-polarization to allow the determination of the absorption coefficient from the crystal spectrum; so instead we use the solution data reported by Brint and McCaffery,[9] who report the spectrum of the tetrabutyl ammonium salt in a polymer matrix at $\sim$10 K. Their data give $\epsilon_{max}$ = 31 $mol^{-1}$ $cm^{-1}$ $dm^3$ and a fwhm line width of 80 $cm^{-1}$, from which the oscillator strength is $1.14 \times 10^{-5}$. After allowing for the orientation average in the polymer solution, we calculate the ratio of the intensity in the $\pi$-polarization to that in the $\sigma$-polarization is $3.4 \times 10^{-4}$.

The transition moments may be expressed as follows:

$$\mu_e = e\sum_i r_i = -(e\hbar/2\pi m\bar{\nu}c)\sum_i \nabla_i$$

$$\mu_m = (e/2mc)\sum_i r \times p_i = (e\hbar/2mci)\sum_i r \times \nabla_i$$

Here $\mu_e$ and $\mu_m$ are the electric and magnetic dipole transition moment operators, $\bar{\nu}$ is the frequency of the transition in wavenumbers, the summation is over all electrons, and we have used a well-known identity connecting the electric dipole and linear momentum operators. If the two excitonic wave functions $\psi_\pm = 1/\sqrt{2}(\phi_1 \pm \phi_2)$ describe in-phase and out-of-phase combinations of single-center one-electron excited states, then we may write

$$\mu_e = -(e\hbar/2m\bar{\nu}c)\langle\psi_+|\nabla|0\rangle$$

and

$$\mu_m = (e\hbar/2mci)\langle\psi_-|r \times \nabla|0\rangle$$

where $|0\rangle$ represents the ground state. The relative magnitude of the transition probabilities is then given by

$$|\mu_m|^2/|\mu_e|^2 = \pi^2\bar{\nu}^2r^2 \qquad (1)$$

With the origin at the center of the rhombohedral unit cell, $r$ is equal to $c/4$ = 487.8 pm, where $c$ is the hexagonal unit cell parameter. Using this distance and the transition frequency of 21 694 $cm^{-1}$ in eq 1 gives a ratio of intensities between the $\pi$- and $\sigma$-polarizations of $1.1 \times 10^{-3}$. Because of the neglect of local field corrections, and the use of data from two different media, this figure appears to be sufficiently close to the observed ratio of $3.4 \times 10^{-4}$ to support this model of the $\pi$-polarized intensity.

**Vibronic Coupling**

The accurate location of the electronic origins provides a good opportunity to unravel much of the vibrational structure in the spectrum. Table II shows the frequencies of a large number of the ground-state fundamentals. These values have been determined from a number of careful studies, involving both infrared and Raman spectroscopy and also $^{15}N$ and $^{18}O$ substitution.[10] Many of the modes are forbidden in the vibrational spectra but can be observed as vibronic sidebands. Figure 7 shows diagrams of the internal modes of the molecular anion. We consider each

(10) Bullock, J. I.; Parrett, F. W. *Can. J. Chem.* **1970**, *48*, 3095. Gatehouse, B. M.; Comyns, A. E. *J. Chem. Soc.* **1958**, 3965. Topping, G. *Spectrochim. Acta* **1965**, *21*, 1743. Woodwark, D. R. D. Phil. Thesis, Oxford, U.K., 1977.

symmetry class in turn. The frequencies of the modes in the various excited states are included in Table II.

The $a_2'$ modes, $\nu_8$–$\nu_{10}$, are readily identified in combination with origin VI, whose $A_1''(D_{3h})$ symmetry ensures that they are the main features in OPA-$\pi$. $\nu_8$ is easily characterized by its $^{15}N$ isotope shift.[11] $\nu_9$ couples weakly to origin VI as expected for a motion of terminal oxygen atoms; on the other hand, $\nu_{10}$ with a frequency of 220.1 $cm^{-1}$ couples very strongly with origin VI. This mode involves the asymmetric stretching of the bidentate oxygen atoms, a motion which enhances the trigonal, acentric component of the equatorial ligand field, in relation to the approximately hexagonal equilibrium distribution of these oxygen atoms. Later we show that this state includes a configuration in which the excited electron is in those f-orbitals that are capable of forming $\sigma$-bonds to the equatorial atoms, so the efficiency of this mode is not surprising.

The $a_1'$ modes are also readily located. Both $\nu_1$ and $\nu_6$ dominate the progressions, and we have discussed their role previously. There is no sign of $\nu_4$ in the optical spectrum, because the terminal oxygen bond stretching does not significantly couple to the electronic excitation. However, both $\nu_5$ and $\nu_7$ appear clearly in OPA-$\pi$ on origin VII (Figure 4), which, having $A_2''(D_{3h})$ symmetry, is itself allowed in this polarization. The latter is the totally symmetric stretching of the uranium to nitrate oxygen bonds. Its frequency, 227.4 $cm^{-1}$, is slightly higher than the asymmetric stretch of the same bonds in $\nu_{10}$. We have also established unequivocally that the corresponding mode in an excited state of the neptunyl(VI) ion has a frequency of 226.4 $cm^{-1}$.[12] The Huang–Rhys factor for this vibration on origin VII is small (Figure 4) and shows that the electronic excitation does not significantly weaken the bonding to the nitrate ions.

There are three modes of $a_2''$ symmetry. All are difficult to observe. In $D_{3h}$ they are forbidden in OPA-$\pi$ for the excited-state symmetries encountered here, while their occurrence in the $\sigma$-polarization is easily masked by the very strong general absorption. The $UO_2$ asymmetric stretch $\nu_2$ can be detected weakly on origins III and VI at 721 and 736 $cm^{-1}$ respectively, as a result of $D_3$ selection rules. There is also evidence for the presence of two quanta of this mode at 23 157 $cm^{-1}$ on origin II, the most convincing being a 0.4-$cm^{-1}$ uranium-235/238 isotope shift observed in the early Manhattan project work on this compound.[13] Variations in this frequency between the excited states appear to follow the variations in $\nu_1$, reflecting changes in the U–O force constants. Of the remaining modes, $\nu_{20}$–$\nu_{22}$, it is only possible to be confident about the frequency of $\nu_{20}$, which appears clearly and strongly, with the correct $^{15}N$ isotope shift, on origin I in the $\sigma$-polarization, as predicted by $D_{3h}$ selection rules.

Most of the e'' modes can be located. $\nu_{23}$, which has a characteristic $^{15}N$ isotope shift, appears in the OPA-$\sigma$ spectrum on origin VII following $D_{3h}$ selection rules. $\nu_{26}$ has a characteristic $^{18}O$ isotope shift and occurs near 186 $cm^{-1}$ on most excited states. It is particularly apparent in TPA. Finally, a sharp feature 164.3 $cm^{-1}$ above origin I in OPA-$\sigma$ clearly combines with $\nu_{26}$ at 186.7 $cm^{-1}$ on the same origin band to give a combination band in the $\pi$-polarization at 352 $cm^{-1}$, as required by e'' symmetry. There is a 1-$cm^{-1}$ $^{15}N$ isotope shift on the combination band which leads to the assignment of $\nu_{24}$ to this frequency, because the only other candidate is the nitrate out-of-plane torsional mode in which the nitrogen atom is not displaced.

There remain nine e' modes to be assigned. The most satisfactory assignments come from $\pi$-polarized intensity on origin I, for which only modes of this symmetry are effective in $D_{3h}$. $\nu_{11}$ and $\nu_{15}$, in common with other terminal N–O modes, are not observed, nor is $\nu_{12}$, but $\nu_{13}$ is present. It has no $^{18}O$ isotope shift and a $^{15}N$ shift of −1 $cm^{-1}$, so its assignment is unambiguous. This mode can also be found on origin VI in TPA. $\nu_{16}$ occurs on this origin with the correct $^{15}N$ isotope shift and is also seen on origin II in the TPA spectrum (Figure 1). $\nu_3$, $\nu_{14}$, and $\nu_{17}$ all occur between 200 and 260 $cm^{-1}$ on origin I. The $UO_2$ bending mode, $\nu_3$, is found at 214 $cm^{-1}$ and is identified by a −10.5-$cm^{-1}$ vibrational isotope shift, which is the correct magnitude for this mode.[14] The other modes occur at 255 and 242 $cm^{-1}$ and show much smaller $^{18}O$ shifts of 2 and 5 $cm^{-1}$, respectively, indicating appreciable mixing with the oxygen bending mode. They are both uranium nitrate stretches, and by analogy to $\nu_7$ and $\nu_{10}$ the symmetric stretch, $\nu_{14}$, is attributed the higher 255-$cm^{-1}$ frequency. $\nu_{18}$, the in-plane deformation of complete nitrate groups, should have a frequency well below the uranium nitrate stretches and less than 200 $cm^{-1}$. There is no evidence for this in the electronic spectrum, but it may be responsible for the very intense Raman band at 151 $cm^{-1}$. The only other internal modes which could account for this are $\nu_{24}$ and $\nu_{25}$.

This discussion illustrates the large information content available in the vibronic spectrum. The results are summarized in Table II. The data confirm that the nitrate internal modes are almost unaltered by the electronic excitations, and the only major changes in frequency involve the modes of the uranyl ion.

Some of the vibrations show splitting or dispersion in conjunction with the electronic transitions, notably $\nu_8$, which is very prominent in OPA-$\pi$ near 23 550 $cm^{-1}$ (Figure 2) and near 27 880 $cm^{-1}$ (Figure 4). Both of these features are composed of a primary peak and satellites which appear 7.6 and 37 $cm^{-1}$ on its high-energy side. Exactly the same substructure intervals appear on $\nu_{16}$ in OPA-$\sigma$ on origin II. These modes differ only in the relative phase of the vibrations in the three chelate rings but both involve the asymmetric stretching of the nitrogen to bridging oxygen bonds. It seems likely that the two strongest components represent a factor group splitting, as a result of the coupling of these vibrations between the two molecules in the unit cell. Combinations of both parities are allowed in the vibronic spectrum, in combination with the exciton states of opposite parity. It will be recalled that the separation between these oxygen atoms in adjacent molecules is 350 pm and is not much larger than the sum of the van der Waals radii, 280 pm.

Finally, we comment on the sharp vibronic structure occurring at frequencies below 150 $cm^{-1}$, which can be seen quite clearly on origin VII in OPA-$\pi$. Bands are found at 21, 30, 34, 48, 74, 95, and 113 $cm^{-1}$. Exactly the same pattern of sharp features is found close to origin II in OPA-$\sigma$ and origin I in TPA. Since this structure is associated with strongly allowed origins, we assume that it corresponds to totally symmetric lattice modes. Although we cannot identify it, one of these modes must correspond to the symmetric response of the axial cesium atoms to the lengthening of the uranium–oxygen bond.

**Table VIII.** Optimized Parameters Values ($cm^{-1}$)

| | $Cs_2UO_2Cl_4$ | $CsUO_2(NO_3)_3$ |
|---|---|---|
| $W_{\sigma\delta}$ | 25 505 | 26 206 |
| $W_{\sigma\sigma} - W_{\sigma\delta}$ | −24 943 | −25 683 |
| $W_{\sigma\phi} - W_{\sigma\delta}$ | 2 065 | 2 296 |
| $W_{\sigma\pi} - W_{\sigma\delta}$ | 14 640 | 15 792 |
| $K_{\sigma\delta}$ | 2 932 | 2 796 |
| $K_{\sigma\phi}$ (=$K_{\sigma\pi}$) | 2 261 | 1 388 |
| $\zeta$ | 1 857 | 1 860 |
| $V_{22}{}^a$ | −431 | |
| $V_{31}{}^a$ | −1 752 | |
| $V_{33}{}^a$ | | 2 510 |
| $\langle B_4\rangle^a$ | 2 696 | |
| $\langle B_6\rangle^a$ | 2 720 | 2 730 |

[a] See ref 12 for parameter notation.

## Electronic Structure

Table VII summarizes the main observables for the nine excited states which can be detected. We can now examine whether the theoretical model which we proposed previously[3] is capable of a

(11) Denning, R. G.; Short, I. G.; Woodwark, D. R. *Mol. Phys.* **1980**, *39*, 1281.
(12) Denning, R. G.; Norris, J. O. W.; Brown, D. *Mol. Phys.* **1982**, *46*, 287.
(13) Dieke, G. H.; Duncan, A. B. F. *Spectroscopic Properties of Uranium Compounds*; McGraw-Hill: New York, 1949.
(14) Denning, R. G.; Snellgrove, T. R.; Woodwark, D. R. *Mol. Phys.* **1976**, *32*, 419.

**Table IX.** Calculated and Observed States of $CsUO_2(NO_3)_3$

| | observed | | | calculated | | | | |
|---|---|---|---|---|---|---|---|---|
| | | | | sym | | | | |
| origin | sym $D_{3h}$ | energy/cm$^{-1}$ | moment/$\mu_B$ | $D_{\infty h}$ | $D_{3h}$ | energy/cm$^{-1}$ | error/cm$^{-1}$ | moment/$\mu_B$ |
| I | E″ | 21089.6 | 0.01 | $\Pi_g$ | E″ | 21151 | +61 | 0.02 |
| II | E′ | 21694 | 1.1 | $\Pi_g$ | E′ | 21708 | +14 | 1.42 |
| III | $A_1''$ | 22307 | | $\Phi_g$ | $A_1''$ | 22285 | -21 | |
| IV | $A_2''$ | 23265 | | $\Phi_g$ | $A_2''$ | 23131 | -134 | |
| V | E′ | 23474 | ~0.3 | $\Delta_g$ | E′ | 23568 | +94 | 1.04 |
| VI | $A_1''$ | 26644 | | $\Phi_g$ | $A_1''$ | 26552 | -92 | |
| VII | $A_2''$ | 27480 | | $\Phi_g$ | $A_2''$ | 27599 | +119 | |
| VIII[a] | E′ | 29618 | >0 | $\Delta_g$ | E′ | 29585 | -33 | 0.05 |
| IX[a] | E′ | 31262 | >0 | $\Gamma_g$ | E′ | 31275 | +13 | 2.39 |
| (X) | | | | $\Phi_g$ | $A_2''$ | 31544 | | |
| (XI) | | | | $\Phi_g$ | $A_1''$ | 33436 | | |

[a] The composition of VIII is 71% $\Delta_g$, 29% $\Gamma_g$. IX is 40% $\Delta_g$, 60% $\Gamma_g$.

satisfactory explanation of the additional data available from this work. Table VIII shows the parameter set found to give the most satisfactory account of the observations. Details of the Hamiltonian operator can be found in refs 3 and 12. In Table VIII the $W_{\alpha\alpha'}$ values define the center of gravity of the various configurations, while the $K_{\alpha\alpha'}$ values are electron-electron repulsion exchange integrals and $V_{33}$ parametrizes the even part of the trigonal field perturbation. Of these parameters $W_{\sigma\delta}$ and $W_{\sigma\sigma} - W_{\sigma\delta}$ serve to establish the correct location of the excited-state manifold in relation to the ground state and are not therefore significant in determining the success of the parametrization. Similarly $W_{\sigma\pi} - W_{\sigma\delta}$ determines the location of states which are not observed in this experiment; because the properties of the other states are only weakly dependent on this parameter, it was fixed at a value found to account for the spectrum of the corresponding neptunyl(VI) compound, where the $f_\pi$ excited states can be observed directly.[12]

Careful consideration of the relative magnitude of $K_{\sigma\phi}$ and $K_{\sigma\pi}$ suggests that the dominant one-center contribution to these integrals is almost identical, so we set them equal.[15] This is not a serious approximation, since $K_{\sigma\pi}$ describes states beyond the range of our experiment and affects the observed levels only in the second order. The optimization therefore uses six parameters to determine eight spectral intervals, between nine excited states. However it is much more tightly constrained than these figures alone indicate, on account of the requirement that the calculated states match the observed ones not only in energy but also in symmetry.

The results of this calculation are contained in Figure 8, which shows the perturbations of the spin–orbit interaction, the electron-electron repulsion, and the trigonal field potential, applied sequentially from left to right. The agreement with the experimental levels is generally good; calculated energies are compared with the experimental values in Table IX. This calculation represents a major advance on our previous attempts to describe this system,[3] by correctly positioning the two new states, VIII and IX, detected by TPA, near 30000 cm$^{-1}$, and properly incorporating the role of the unobserved $\sigma\pi$ configuration.

It is striking that the MCD spectrum of Brint and McCaffery[8] shows a very small positive $A$ term for origin VIII and a much larger one of the same sign for origin IX, in good agreement with the figures for the magnetic moments included in Figure 8. Furthermore the two states show large MCD $B$ terms of opposite sign, indicative of a large second-order Zeeman interaction linking them.

The source of the MCD can be understood by examining Figure 8, which shows that in the cylindrical field, illustrated in the center of the diagram, the $\Gamma(\sigma\phi_{7/2})$ state has a first-order magnetic moment of 5.0 $\mu_B$ and that it is very close to an accompanying $\Delta$ state with predominantly $\sigma\delta_{5/2}$ parentage. However, because of the second-order spin–orbit interaction, which has already been diagonalized at this point, the latter also contains a major $\sigma\phi_{5/2}$

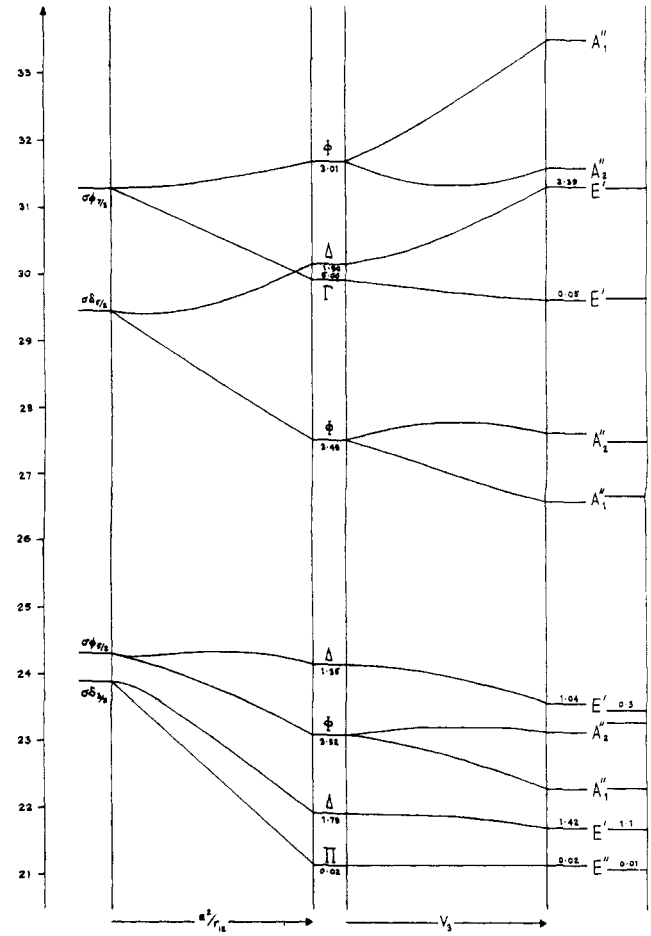


**Figure 8.** Calculated and observed energy levels for $CsUO_2(NO_3)_3$, showing sequential perturbations. Numbers on the levels indicate magnetic moments in Bohr magnetons ($\mu_B$).

contribution. This component is strongly mixed by the trigonal field with the $\Gamma(\sigma\phi_{7/2})$ state, with which it is nearly degenerate, so that the two states near 30000 cm$^{-1}$ appear to repel one another when the trigonal field is applied; their composition is shown in the footnote to Table IX. As a result the original very large magnetic moment, 5.0 $\mu_B$, of the $\Gamma$ state becomes off-diagonal, connecting the two final states which are responsible for origins VIII and IX and introduces opposite-signed MCD $B$ terms into the two origin bands. The magnitude of the residual first-order moment which is responsible for the MCD $A$ terms in the two states is clearly very sensitive to the details of the energy level scheme and in particular to the magnitude of the trigonal field, which redistributes the moments. This satisfactory qualitative account of the MCD spectrum therefore gives a strong indication of the quality of the Hamiltonian. It is not practicable to undertake a more quantitative analysis of the MCD spectrum, be-

(15) Barker, T. J. D. Phil. Thesis, Oxford, U.K., 1990.

cause of the large number of overlapping components in the spectrum.

Table VIII also includes the parameters which best describe the data on $Cs_2UO_2Cl_4$ which we reported in part I. It is clear that, apart from the equatorial field, both sets are closely comparable and that the description of the electronic structure in terms of a linear triatomic uranyl ion, weakly perturbed by the equatorial ligands, is a valid one. The only major difference between the two parameter sets is in $K_{\sigma\phi}$; the smaller value in $CsUO_2(NO_3)_3$ could be related to the presence of $\sigma$-bonding in the $f_\phi$ orbital set, which is absent in $Cs_2UO_2Cl_4$. It is also interesting but probably fortuitous that the radial parameter derived from a point charge potential expansion using actual ligand geometries,[12] $\langle B_6 \rangle = eq\langle r^6 \rangle / R^7$, where $q$ is the charge on each coordinated atom in the equatorial plane, is essentially identical for both compounds.

The configurations responsible for the observed excited states are $\sigma\delta$ and $\sigma\phi$. It is the splitting of the $f_\phi$ orbitals by the trigonal field which dominates the equatorial field perturbation in $CsUO_2(NO_3)_3$. One of these is $\sigma$-antibonding with respect to the nitrate oxygens while the other is nonbonding. It is therefore easy to understand why the in-phase asymmetric stretching of the uranium bidentate oxygen bonds, $\nu_{10}$, illustrated in Figure 7 is so effective at introducing intensity in conjunction with origin VI, producing the one strong OPA feature in Figure 3, because this excited state includes a large contribution from the $\sigma\phi$ configuration. Regarding the coordination sphere as a hexagon of oxygen atoms, $\nu_{10}$ shortens a bond in the $+x$ direction while lengthening a bond in the $-x$ direction, a perturbation that strongly mixes orbitals of *gerade* symmetry with the *ungerade* f-orbitals.

## Conclusion

We have shown that TPA is a valuable adjunct to OPA for electronic excitations which are intrinsically parity conserving, even when the site symmetry of the chromophore is noncentric. The two types of experiment can be complementary in their selection rules and in their emphasis on vibronic structure. Here they are sufficient to establish an unequivocal assignment of the location and symmetry of eight excited states and to determine the location of a ninth (origin IV) to within about 20 $cm^{-1}$. The detail of the analysis makes it possible to identify an example of a transition which is magnetic dipole allowed as a result of the excitonic (or Davydov) coupling of electric dipole allowed single-center transitions. Magnetic dipole transition moments arising from coupled oscillators are more commonly manifest in the natural circular dichroism of chiral chelate complexes and helical polymers.

The quality of the data makes it possible to test the nature of the excited-state configurations in $CsUO_2(NO_3)_3$ semiquantitively through an empirical parametrization, and we conclude that the component configurations are closely similar to those which describe the excited states of $Cs_2UO_2Cl_4$.[3] These configurations are those in which a $\sigma_u$ electron is promoted from the HOMO to a set of LUMO's composed of uranium f-orbitals in the energy order $f_\delta < f_\phi \ll f_\pi \ll f_\sigma$. We have recently reviewed the ability of MO calculations, at various levels of sophistication, to match these observations[16] and note that the occurrence of a $\sigma_u$ HOMO is strongly influenced by the underlying pseudocore 6p-shell, whose participation in the bonding appears crucial in determining the stable trans geometry of the uranyl ion.[16,17] We have termed this phenomenon, which appears to have some general validity, the inverse trans influence.[16]

**Acknowledgment.** We are indebted to the Science and Engineering Research Council for the support of T.J.B. and J.R.G.T. and to the staff of the Laser Support Facility at the Rutherford Appleton Laboratory for invaluable assistance. We also wish to thank I. D. Morrison for assistance with the data handling.

(16) Denning, R. G. *Struct. and Bonding*, in press.
(17) Tatsumi, K.; Hoffmann, R. *Inorg. Chem.* **1980**, *19*, 2656.

Contribution from the Department of Chemistry, Mudd Building No. 6, Lehigh University, Bethlehem, Pennsylvania 18015

# Relaxation Enhancement of Water Protons by Manganese(III) Porphyrins: Influence of Porphyrin Aggregation

Kenneth E. Kellar and Natalie Foster*

*Received June 11, 1991*

The ability of eight manganese(III) porphyrins to enhance the longitudinal relaxation rate of water protons in aqueous solution has been studied by nuclear magnetic resonance dispersion (NMRD). In NMRD, the relaxation rates of solvent water protons are measured as a function of proton Larmor frequency from 0.01 to 50 MHz (field strengths from 0.23 mT to 1.17 T); a plot of relaxation rate versus frequency is called an NMRD profile. To enable comparison of the data, the observed rates are expressed as relaxivities by normalizing the rates to the concentration of manganese(III) porphyrin. Five porphyrins exhibited similar profiles characterized by high relaxivities, while the profiles for three porphyrins were different and demonstrated much lower relaxivities. Analysis of the NMRD profiles by relaxation theory yields correlation times, the values of which are sensitive to interactions between the hydrated manganese(III) porphyrin and its environment. The values of some correlation times for the three porphyrins with low relaxivities were inconsistent with those showing high relaxivities. Because the values of these correlation times indicate that interactions are occurring between manganese atoms and because differences in structure are apparent between the three porphyrins with lower relaxivities and the five with high relaxivities, it is hypothesized that the three porphyrins exist as aggregates in solution while the others exist as monomers. Addition of perdeuterated acetone to solutions of the porphyrins with low relaxivities caused them to attain relaxivities that are similar in magnitude to the others at all frequencies, while the addition of acetone to solutions of porphyrins with high relaxivities causes no significant change in their relaxivities. Because the addition of acetone is known to break up porphyrin aggregates, the assertion that aggregation is directly responsible for the low relaxivities in aqueous solution is strongly supported.

## Introduction

The addition of a manganese(III) porphyrin to water causes an increase in the longitudinal relaxation rate of the water protons.[1,2] This increase in the relaxation rate normalized to the concentration of the porphyrin is called the relaxivity of the porphyrin. Investigators have shown that manganese porphyrins generally have what is considered a high relaxivity, typically about 9 $mM^{-1}$ $s^{-1}$ at 37 °C and 20 MHz.[3,4] This corresponds to about

* To whom correspondence should be addressed.

(1) Chen, C.-W.; Cohen, J. S.; Myers, C. E.; Sohn, M. *FEBS Lett.* **1984**, *168*, 70.
(2) Koenig, S. H.; Brown, R. D., III; Spiller, M. *Magn. Reson. Med.* **1987**, *4*, 252.

0020-1669/92/1331-1353$03.00/0 